Signal enhancement ratio imaging of the lung parenchyma with ultra-fast steady-state free precession MRI at 1.5T

Orso Pusterla, MSc *[1,2]; Gregor Sommer, MD, MSc *[3]; Francesco Santini, PhD [1,2]; Mark Wiese, MD [4]; Didier Lardinois, MD [4]; Michael Tamm, MD [5]; Jens Bremerich, MD, MHBA[3]; Grzegorz Bauman, PhD [1,2]; Oliver Bieri, PhD [1,2]

* These authors contributed equally to this work and share first authorship.

[1]Division of Radiological Physics, Department of Radiology, University Hospital of Basel, Basel, Switzerland
[2]Department of Biomedical Engineering, University of Basel, Basel, Switzerland
[3]Clinic of Radiology and Nuclear Medicine, Cardiac and Thoracic Imaging, University Hospital of Basel, Basel, Switzerland
[4]Clinic of Thoracic Surgery, University Hospital of Basel, Basel, Switzerland
[5]Clinic of Pneumology, University Hospital of Basel, Basel, Switzerland

Published in the **Journal of Magnetic Resonance Imaging** as an *Original Research Article.*

Main Body: Abstract 300 words; Body 3800 words; 7 Figures; 3 Tables; 40 References.

Supporting Material for review and online publication**:** 5 Supporting Figures (included in 1 pdf document).

Corresponding author:
Orso Pusterla, MSc ETH in Physics
Division of Radiological Physics, Department of Radiology
University Hospital of Basel
Petersgraben 4, CH-4031 Basel, Switzerland
E-mail: orso.pusterla@unibas.ch
Phone: +41.61.558.51.77

ACKNOWLEDGEMENTS

This work was supported by the Swiss National Science Foundation (SNF grant No. 320030_149576) and by a Seed Grant of the International Society for Magnetic Resonance in Medicine (ISMRM) 2014. The funders had no role in study design, data collection and analysis, decision to publish, or preparation of the manuscript.

Running Title: SER imaging of the lung parenchyma.

ABSTRACT

Background: Lung perfusion MRI after i.v. Gd-administration is commonly based on spoiled gradient-echo acquisitions, such as volume-interpolated breath-hold examinations (VIBE), suffering from low signal-to-noise in the parenchyma.

Purpose: To investigate the lung signal enhancement ratio (SER) with ultra-fast steady-state free precession (ufSSFP) after Gd-administration.

Study Type: Retrospective.

Subjects: Ten subjects with healthy lungs; nine patients with pulmonary diseases (COPD, lung cancer, pulmonary fibrosis, lung contusion).

Field Strength/Sequence: VIBE and ufSSFP imaging of the chest was performed at 1.5T before and three minutes after i.v. Gadobenate-Dimeglumine.

Assessment: A workflow including deformable image registration and median filtering was used to compute 3D SER maps. SER was analyzed in the lung, blood pool, liver, muscles, and fat. The artifacts were assessed by a radiologist. In the COPD patients, ufSSFP-SER was compared to ^{99m}Tc-MAA-SPECT/CT by visual scoring of lung enhancement deficits.

Statistical Tests: Mean signal, standard deviation (SD), intersubject SD, and coefficient of variation (cv) were calculated for SER. Statistical significance of differences in signal and artifacts were determined using Wilcoxon signed-rank paired

test. Intermodality agreement between ufSSFP-SER and SPECT/CT was calculated by Cohen's kappa (κ_q).

Results: In healthy lungs, ufSSFP-SER (99%±23%, mean±pooled intrasubject SD, cv=23%) was significantly higher ($P<10^{-3}$) and more homogeneous ($P<10^{-3}$) than VIBE (47%±26%, cv=57%). UfSSFP-SER was significantly higher ($P<10^{-3}$) for the lungs (99%±9%, mean±intersubject SD) than for the blood (81%±7%) and other tissues (liver 33%±8%, muscle 26%±5%, fat 2%±1%). In the lung ufSSFP-SER exhibits homogeneity on iso-gravitational planes, and an anterior-posterior gradient.

In COPD patients, ufSSFP-SER was reduced and less homogeneous compared to the control group (73%±33%, mean±pooled intrasubject SD, cv=42%). UfSSFP-SER had moderate intermodality agreement with SPECT/CT (κ_q = 0.64).

Data Conclusion: UfSSFP-SER of the lung is a rapid and simple method. Our preliminary data show plausible results in different pulmonary diseases, motivating further evaluation in larger cohorts.

Keywords: Magnetic Resonance Imaging; Steady-State Free Precession; Contrast Agent; Methods Development; Pulmonary Disease; Lung MRI.

Running Title: SER imaging of the lung parenchyma.

INTRODUCTION

Pulmonary diseases are an important burden to public health (1, 2). Functional information on pulmonary perfusion obtained from diagnostic imaging plays a pivotal role for patient management, both in terms of diagnosis and therapy planning (2–4). Pulmonary perfusion is commonly assessed by scintigraphy and hybrid single photon emission tomography/computed tomography (SPECT/CT) using ^{99m}Tc-labelled macro-aggregated albumin (MAA) (4). Alternatively, contrast-enhanced dual-energy CT (5) can be performed, but is not yet fully established in clinical practice. Similarly, magnetic resonance imaging (MRI) has been described as a promising method to assess pulmonary morphology and function (3, 6–9). Since MRI comes without an associated radiation burden (7, 10, 11), further technical development of pulmonary MRI is of interest particularly for frequently repetitive imaging investigations, where radiation protection is an issue.

Functional information about pulmonary perfusion is commonly assessed by MRI from a heavily T1-weighted spoiled gradient-echo (SPGR) in combination with the intravenous injection of a contrast agent (6). Using rapid volumetric SPGR imaging during the wash-in, peak-enhancement, and wash-out of the contrast agent, dynamic contrast-enhanced (DCE) MRI enables to measure both blood-volume and flow (12). Moreover, static contrast-enhanced imaging is conventionally performed with SPGR, such as volume interpolated breath-hold examinations (VIBE) (3, 10). These contrast-enhanced MRI methods have demonstrated to correlate reasonably well with ^{99m}Tc-MAA-SPECT (13), however, with one important limitation: while ^{99m}Tc-MAA-SPECT represents tracer

accumulation in the pulmonary arterioles and capillary bed, i.e. in the pulmonary parenchyma itself (14), gradient-echo imaging is mainly sensitive to larger vessels, and suffers from low signal-to-noise ratio (SNR) in the lung parenchyma (15).

In contrast, balanced steady-state free precession (bSSFP) offers the highest SNR per unit of time amongst all MRI sequences (16). Banding artifacts that typically compromise the image quality of bSSFP in the chest have been recently mitigated by the development of an ultra-fast SSFP imaging approach (ufSSFP) (17); a variant of bSSFP with ultra-short repetition times, which has already demonstrated potential for morphological and functional assessment of the lungs (8, 18–20). Due to their mixed contrast behavior driven by the T2/T1 relaxation time ratio (21), bSSFP sequences are frequently regarded as being rather insensitive to gadolinium-based contrast agents, although their potential use after contrast administration has been demonstrated and advised (22, 23). From the theory (16), the signal enhancement for SSFP after contrast administration is expected to be higher for tissue with long T1 and short T2, such as the lung (T1 / T2 ~ 1375 / 66 [ms] at 1.5T, cf. (24)), as compared to the blood (T1 / T2 ~ 1300 / 300) and fluids with comparable T1 / T2.

The purpose of our work is to investigate the static signal enhancement ratio (SER) of ufSSFP and VIBE from two sets of volumetric scans, acquired before and after the administration of a gadolinium-based contrast agent.

MATERIALS AND METHODS

This study was approved by the local institutional review board and all subjects gave written informed consent. Imaging examinations were performed between July 2015 and December 2016.

Study Subjects

Pulmonary SER imaging with ufSSFP and VIBE was retrospectively evaluated in 10 consecutive patients (4 males, 6 females; mean age 40±13 years, range 25-64) with healthy lungs who received chest MRI with contrast agent because of a suspected mediastinal mass. For structural and functional examination of the lung, both ufSSFP and VIBE sequences were part of our routine clinical MRI protocol.

Mediastinal mass was excluded, through MRI in eight cases. One subject had thymic hyperplasia, another subject had an esophageal duplication cyst. Since no disease of the lung was present, these 10 patients are in the following referred to as the “control group” of the study.

Static ufSSFP-SER imaging was further assessed in nine patients with common pulmonary diseases showing a diversified spectrum of pulmonary pathologies. Seven patients (3 males, 4 females; mean age 64±10 years, range 45-74) were examined as part of an ongoing clinical trial investigating the potential of MRI in chronic obstructive pulmonary disease (COPD). Of these seven COPD patients, three patients had COPD global initiative for chronic obstructive lung disease (GOLD) stage II, one patient GOLD stage III, and three patients GOLD stage IV; three of the COPD patients had evident

emphysema and four had non-small-cell lung cancer (NSCLC). In these seven COPD patients, recent ^{99m}Tc-MAA-SPECT/CT exams (delay 21±22 days, interval: 1-51 days) were available for comparison to SER imaging.

Two further patients with a different pulmonary pathology than COPD who were examined with ufSSFP-SER imaging are also included in this study for illustration purposes. The first patient, a 54-year-old female with scleroderma and non-specific interstitial pneumonia (NSIP), received the MRI exam for routine follow-up; in this patient, the morphological MR images were taken for comparison to ufSSFP-SER imaging. The second patient was a 71 years old male with traumatic lung contusion who underwent CT and MRI (interval: 8 days) after a traumatic accident.

MR Imaging

All MRI scans were performed on a whole-body 1.5T MR scanner (MAGNETOM Avanto, Siemens Healthineers, Erlangen, Germany) using a 24-channel spine and a 12-channel thorax receive-array centered on the lungs. Both ufSSFP (17) and VIBE scans were acquired before and after intravenous injection of Gadobenate Dimeglumine (MultiHance®, Bracco Imaging S.p.A., Milan, Italy) using the standard dose of 0.2 ml per kg body-weight. In order to avoid the first pass (concentration peak) of the contrast agent, and rather have a static distribution of contrast (25), post-contrast imaging for static SER mapping was performed 3 minutes after the contrast injection: first with ufSSFP, and immediately after (ca. 30 s) with VIBE, resulting in a similar contrast agent concentration for the two imaging modalities (25).

Imaging with both volumetric sequences was performed in inspiratory breath-hold. The sequence parameters were chosen to obtain a high spatial resolution to guarantee good morphological details for the radiological diagnosis [see Heye et al. (8)] and similar acquisition times (~15 seconds). If necessary, the ufSSFP acquisitions could be shortened by the technician to 11 seconds to minimize the respiratory effort. The repetition time (TR) of the ufSSFP sequence was minimal, to avoid banding artefacts; the TR for VIBE was set as recommended elsewhere (26). The flip angle for ufSSFP and VIBE were set for close-to-maximal lung signal intensity after contrast agent administration, following the theoretical signal-model (27) and as explained elsewhere (23). Due to radiological image preferences, ufSSFP was acquired with coronal and VIBE with transverse image orientation. Detailed parameters for ufSSFP and VIBE are available in Table 1.

SPECT/CT

Lung perfusion SPECT/CT was performed in the seven COPD patients as part of the routine clinical workup using a standard administered dose of 111 MBq ^{99m}Tc-MAA. The scintigraphy and SPECT were acquired on a double-head SPECT/CT scanner (Symbia Intevo 16, Siemens Healthineers, Forchheim, Germany). Three-dimensional ordered subset expectation maximization (OSEM) with 4 subsets, 8 iterations and 4 mm Gaussian filtering was used for reconstruction. The voxel size was isotropic 4.8 mm. The acquisition time for SPECT was 20 min. The CT scans followed a low dose protocol with 130 kV and 30 mAs reference values resulting in a total dose-length product (DLP)

of ~100 mGycm. CT-data were reconstructed using filtered back projection with a B70s convolution kernel. The slice thickness was 1.5 mm and the in-plane resolution was 0.7×0.7 mm^2.

MR Image Post-processing

Pre- and post-contrast volumetric datasets were first co-registered to spatially match lung structures, such as vessels and lung boundaries, using a mass preserving three-dimensional deformable B-spline image registration algorithm (Elastix version 4.7, University Medical Center Utrecht, The Netherlands) (28). Subsequently, the registered datasets were median filtered (kernel radius 9×9×9 mm^3). Median filtering [see Ref. (29) for details], a common edge-preserving noise reduction filter, is particularly effective to remove “salt and pepper” type of noise, that is sparsely occurring white and black pixels, such as the hyperintense vasculature overlying the pulmonary tissue and small airways (up to a size of 9×9×9 mm^3 in our post-processing). Finally, SER images were calculated voxel-wise (at position $\vec{x}$) from the signal intensity before [$SI_{pre}(\vec{x})$] and after [$SI_{post}(\vec{x})$] contrast agent administration, respectively, using

$$SER(\vec{x}) = \frac{SI_{post}(\vec{x}) - SI_{pre}(\vec{x})}{SI_{pre}(\vec{x})}.$$

Image post-processing was identical for ufSSFP and VIBE, and essentially similar to previous works (19, 20). Signal preservation by the image registration was analyzed by comparing the whole-lung signal before and after image registration.

A schematic summary of the proposed method is shown in the Supporting Figure S1.

Visual and Quantitative Data Analysis

To analyze the difference between VIBE and ufSSFP-SER imaging, five volumetric regions of interest (ROI) were manually segmented in every subject comprising the whole lung (excluding large vessels), the aortic-arch blood pool, the whole liver (excluding large vessels), muscles (subscapularis, pectoralis), and subcutaneous thoracic fat. Supporting Figure S2 shows an exemplary segmentation of these ROIs. For every ROI and every individual, the mean value and standard deviation (SD) of the SER were computed. From these, the group mean, the intersubject SD (interindividual deviation from the group mean) and pooled intrasubject SD (square root of the average variance) were calculated. The coefficient of variation (ratio of pooled intrasubject SD and group mean) was also calculated for the lung ROI. Statistical significances were determined using Wilcoxon signed-rank paired test.

The robustness (artifact behavior) of SER imaging was assessed in the control cohort by a board certified radiologist and nuclear medicine physician (G.S., 9 years of clinical experience). The radiologist scored on the SER images, for every lung lobe, the percentage of volume affected by artifacts (score 0, no artifacts; score 1, 1-25% of lobe volume; score 2, 26-50%; score 3, 51-75 %; and score 4, 76-100%). Statistical significance between ufSSFP-SER and VIBE-SER artifact scoring was determined using Wilcoxon signed-rank paired test.

For the COPD patients, ufSSFP-SER of the lung was compared to ^{99m}Tc-MAA-SPECT/CT. To this end, a radiologist and nuclear medicine physician (G.S.) visually

scored on SPECT/CT, for every lung lobe, the extent of visible perfusion deficits as percentage of the lobar volume (score 0, no defects; score 1, 1-25% of lobe volume affected; score 2, 26-50%; score 3, 51-75%; score 4, 76-100%). The same scoring was performed for the ufSSFP-SER images by a second board certified radiologist (J.B., 20 years of clinical experience). Intermodality agreement was calculated by Cohen's kappa coefficient using both linear and quadratic weighting (κ_l and κ_q, respectively) (30, 31).

For the NSIP and the trauma patients, ufSSFP-SER images were visually correlated with morphological MR and / or CT by a radiologist (G.S.).

Image post-processing and statistical analysis were performed with Matlab (Mathworks, Natick, MA, USA) by three physicists experienced in medical imaging (O.P., G.B. and F.S., with 3, 9 and 11 years of experience).

RESULTS

Signal Enhancement in the Control Group

In all subjects, ufSSFP and VIBE scans provided diagnostic image quality and allowed the derivation of static, volumetric, SER images. Imaging was performed in inspiratory breath-holding and thus in similar breathing phases. As a result, image registration was successful in all cases. Lung signal intensity was not affected by the registration, deviating by -2.7% to 2.9% (min, max) for ufSSFP (mean±SD = 0.8%±1.9%), and by -5.4% to 6.2% (0.3%±4.3%) for VIBE. No patient was excluded from the analysis.

A side-by-side comparison of ufSSFP and VIBE pre- and post-contrast images (maximum intensity projection) is presented in Figure 1 for a representative subject from the control cohort (no lung disease). As compared to non-enhanced imaging (Figs. 1a and c), after contrast administration both VIBE and ufSSFP show a clear signal increase in the lung parenchyma and vasculature (Figs. 1b and d), also yielding enhanced morphological details. In both pre- and post-contrast imaging with ufSSFP the signal of fine vessels and parenchyma is clearly caught until the very periphery of the lung (Figs. 1a and b); especially when compared to the dark background signal of the trachea. In contrast, with VIBE almost similar signals are registered in the lung periphery and trachea.

Figure 2 shows, for a subject of the healthy cohort, native ufSSFP and VIBE images pre- and post-contrast together with the resulting static SER images. The efficacy of median filtering on the same data is exemplary shown in Supporting Figure S3. In this

subject (Fig. 2), the average lung SER using ufSSFP (Fig. 2c) was 96%±23% (mean±SD), appearing homogeneous on iso-gravitational planes (e.g. 95%±13% on the presented coronal slice in Fig. 2c), but revealing an increase from non-dependent (ventral, e.g. 83%±19%) to dependent areas (dorsal, e.g. 114%±19), as expected in a healthy lung. In contrast, VIBE-based SER images of the same subject (Fig. 2f) appear highly inhomogeneous with a considerably lower mean whole lung SER of 41%±28%. Similar results are found for all the subjects of the control group. Supporting Figure S4 shows additional comparisons between ufSSFP-SER and VIBE-SER imaging (similarly to Figs. 2c and 2f) in three other subjects from the control group.

For the ten subjects of the control cohort, group-averaged SER values are outlined in Table 2 for different anatomical regions. For ufSSFP, the SER values were significantly higher in the lung parenchyma (99%±9%, mean±intersubject SD) than in the blood pool (81%±7%, $P<10^{-3}$) and in other tissues (liver 33%±8%, muscle 26%±5%, fat 2%±1%). As a consequence, ufSSFP-SER images reveal an improved depiction of the lung parenchyma (cf. Fig. 2c). In contrast, VIBE-based SER of the lung was significantly lower ($P<10^{-3}$) and more inhomogeneous (mean=47%, pooled intrasubject SD=27%, cv=57%, $P<10^{-3}$), as compared to ufSSFP-SER (mean=99%, pooled intrasubject SD=23%, cv=23%). In the blood pool, however, VIBE-SER (164%±17%, mean±intersubject SD, $P<10^{-3}$) was twice as high (ufSSFP-SER, 81%±7%).

A schematic of the artifacts perceived on ufSSFP-SER and on VIBE-SER images is presented in Table 3. Generally, for the control group, ufSSFP-SER images were

broadly homogeneous, revealing only limited image artifacts. Overall, for ufSSFP, none of the SER images had an artifact scoring above 2 (artifact size <50% for every lung lobe). The left lower lobe of the lung was the region most prone to artifacts caused to heart beating and partial volume effects (see e.g. Fig. 2c). In contrast, VIBE-SER of the lung is generally prone to artifacts and signal variations, even in the absence of parenchymal abnormalities. The average score of the artifacts per lobe was 2.3±0.6 for VIBE-SER, and 0.6±0.4 for ufSSFP-SER. The artifact scoring for ufSSFP-SER was significantly lower than for VIBE-SER ($P<10^{-12}$).

Overall, for the purpose of pulmonary SER imaging, ufSSFP outperformed VIBE, providing an accentuated signal enhancement and visually homogeneous SER images (mean=99%, pooled intrasubject SD=23%, cv=23%) with a reduced intersubject standard deviation among the collective of subjects with healthy lung (mean=99%, intersubject SD=9%). As a result, only the static signal enhancement, as observed with ufSSFP, was further investigated for SER imaging in patients with pulmonary disease.

Signal Enhancement in Pathologic Lung Tissue

The radiological potential of ufSSFP-SER imaging of the lung was evaluated in patients with pulmonary diseases including COPD, lung cancer, pulmonary fibrosis, and traumatic lung contusion. UfSSFP imaging was successful for all patients, who could perform the 15s long breath-holding maneuvers.

Side-by-side comparisons of morphological ufSSFP, ufSSFP-SER, and SPECT/CT imaging for three representative COPD patients are shown in Figure 3, Figure 4 and Supporting Figure S5 (COPD GOLD II, COPD GOLD IV, and COPD GOLD III with lung cancer, respectively). In contrast to ufSSFP-SER of the control group (SER = 99%±23%, mean ± pooled intrasubject SD), ufSSFP-SER of the lung in the seven COPD patients was characterized by an overall significantly ($P<10^{-3}$) lower signal enhancement and significantly ($P<10^{-3}$) larger inhomogeneities (SER=73%±33%, mean ± pooled intrasubject SD, cv=42%, intersubject SD=15%). Visually, there was a moderate to strong spatial correspondence between areas of low SER and regions with low radiotracer uptake on ^{99m}Tc-MAA-SPECT (see Fig. 3, Fig. 4 and Supporting Fig. S5). Interestingly, in the patient with NSCLC (Supporting Figure S5) the SER in the tumor (43%±8%) was lower than in the lung parenchyma (68%±24%).

A comparison of the functional defects, assessed for the COPD patients, with ufSSFP-based SER imaging and with SPECT/CT is shown in Figure 5. The lobar scoring for the two imaging modalities shows that SER imaging tends to underestimate the size of defects in COPD compared to SPECT/CT (the mean score of defects in our cohort was 2.0±0.9% for ufSSFP-SER, and 2.5±1.0% for SPECT); Cohen's kappa coefficients indicate moderate intermodality agreement between SPECT/CT and ufSSFP-SER (κ_l=0.41, κ_q = 0.64, fair agreement).

The clinical potential of ufSSFP-based SER imaging is further illustrated in a NSIP and a trauma patient in Figures 6 and 7. In the patient with NSIP (Fig. 6), the fibrotic lung

regions visible on the morphological MR images exhibit a streaky decrease in SER (67%±25%) as compared to the healthy parenchyma (99%±22%; whole lung SER=96%±23%). In the trauma patient (Fig. 7), a hematoma is visible inside the lung parenchyma on CT and post-contrast ufSSFP images; the lesion is also well observable on ufSSFP-based SER maps, and reveals a strongly reduced SER (34%±23%) as compared to the healthy lung (110%±27%).

DISCUSSION

From the shortened TR, as compared to contemporary bSSFP methods (16), ufSSFP (17) offers banding-free chest imaging at 1.5T and has shown promising result for morphological and functional investigations (8, 9, 17–20, 24). In this work, we have extended the prospects of ufSSFP imaging to the diagnosis of functional abnormalities of the pulmonary parenchyma in combination with the administration of an intravenous contrast agent. In contrast to the common consensus that bSSFP sequences are insensitive to contrast agents (16), the ufSSFP signal can be notably increased. In fact, in the post-contrast ufSSFP images, the signal of lung tissue doubles, revealing the highest increase amongst all captured organs and the blood pool.

It might be interesting to note that the signal of coherent SSFP, such as balanced SSFP (and thus ufSSFP), scales with T1/T2 (16, 17, 27), whereas the signal of incoherent SSFP, such as VIBE, is predominantly weighted by T1. From this, especially in the limit of large T1/T2 as for the lung (T1 / T2 ~ 1375 / 66 [ms], cf. (24)), a similar signal enhancement would be expected for both methods. Overall, ufSSFP, however, revealed to be markedly superior to VIBE. This is most likely caused by the low SNR of VIBE for lung tissue, as a result of the rather long echo time (TE) for DCE MRI not being adapted to the short T2* of the lung. As a result, VIBE acquisitions with considerably shortened TE, or alternatively ultra-short echo time sequences (32, 33), might lead to an improvement for lung SER imaging; especially at higher field strength where susceptibilities effects still limit the applicability of ufSSFP (18).

Overall, ufSSFP-SER images provide a highlighted throughout depiction of the lung parenchyma. This is in contrast to SER images derived from VIBE that were flawed even in the control cohort of subjects with no pulmonary disease by prominent signal variations in the absence of parenchymal abnormalities. Moreover, ufSSFP-SER images of healthy lung tissue appeared iso-gravitationally homogeneous, but with a prominent gravitational-related gradient increasing the signal from ventral to dorsal lung, in accordance with literature (34–36). In the COPD patients, ufSSFP-SER images were characterized by marked inhomogeneities, that coincided with the functional defects seen on ^{99m}Tc-MAA-SPECT (moderate intermodality agreement κ). In the NSIP patient, a decrease in SER values was noted for the fibrotic regions of the lung, corresponding well to morphological MR. Similarly, in the trauma patient, the SER images were sensitive in detecting a lung hematoma.

We observed a moderate intermodality agreement between SPECT/CT and static ufSSFP-SER in the lobe-by-lobe evaluation of the COPD patients. This result may be affected by the fact that the methods of image acquisition for SPECT, in free breathing, and for ufSSFP, in breath-hold, differ substantially. Furthermore, while SPECT/CT is known to reflect ^{99m}Tc-MAA lodged in the capillaries (and not in the extravascular parenchyma) thanks to arterial perfusion, the exact anatomic and physiological origin of the signal enhancement observed in the lung with ufSSFP is unknown. From our preliminary data, we hypothesize that this effect is primarily related to the smaller vasculature of both the arterial and venous side of the capillary beds and may additionally include also parenchymal tissue contrast as a sort of “delayed

enhancement". The final answer to this question, however, cannot be given by this feasibility study and requires further investigation.

While the obtained results with ufSSFP-SER imaging in patients appear promising, we acknowledge that the administration of contrast agent might not be indicated for some categories of subjects (e.g. in case of renal failure or allergy). Furthermore, the current approach requires short breath-holding maneuvers, which sometimes may not be feasible (e.g. in infants), but might be overcome by using self-navigated free-breathing methods (37). Similarly, residual motion artifacts spotted on SER images can, in principle, be addressed with cardiac triggered acquisitions, but only at the cost of scanning efficiency.

It may be perceived as a limitation of the present study that the signal enhancement of ufSSFP was not investigated dynamically at several time-points after contrast agent injection, as performed with traditional DCE-MRI. Resolving dynamic contrast enhancement with ufSSFP requires an adaptation of the sequence, e.g., using view-sharing methods (38). This will be subject of future investigation. Another focus of ongoing development will be attempting to suitably standardize the measurement (e.g. hardware, parameters, post processing, reproducibility). In this context quantitative SER imaging might automatically identify lung defects lobe-by-lobe, for instance by using algorithms involving adaptive k-means thresholding (39) of the SER signal-distributions, and segmentation pipelines as presented by Tustison et al. (40) or using machine learning.

Another limitation of our work is that the group of patients with pulmonary pathology is small. Hence, our study only demonstrates the technical feasibility of pulmonary ufSSFP-SER imaging in some of the most common pulmonary disease conditions associated with respiratory discomfort (eight of the included patients, except the trauma patient, had impaired pulmonary function with an FEV1 of 20%-75% of normal). We cannot yet provide any validation of ufSSFP-SER imaging in terms of its diagnostic role for specific diseases. To this end, further prospective investigation of the method in a larger collective of subjects and against standard functional imaging methods, such as DCE-MRI with high temporal resolution and SPECT/CT, is required.

In conclusion, the signal of ufSSFP is increased in the lung parenchyma following intravenous injection of gadolinium-based contrast agents. In combination with a pre-contrast native acquisition and specific post-processing, ufSSFP-based SER imaging offers an improved depiction of the pulmonary parenchyma. Preliminary findings in patients show plausible patterns of signal distribution for different pulmonary diseases. Added as a complement to common contrast-enhanced MRI protocols (e.g. DCE-MRI), ufSSFP-SER imaging may thus provide helpful complementary information about the functional abnormalities of the lung parenchyma from only two rapid breath-hold scans. Its clinical benefit, particularly in comparison to ^{99m}Tc-MAA-SPECT/CT and DCE-MRI, remains to be further investigated.

REFERENCES

1. Bousquet J, Khaltaev NG, Cruz AA: *Global Surveillance, Prevention and Control of Chronic Respiratory Diseases: A Comprehensive Approach*. Geneva : World Health Organization; 2007.

2. Ley-Zaporozhan J, Ley S, Kauczor H-U: Morphological and functional imaging in COPD with CT and MRI: present and future. *Eur Radiol* 2008; 18:510–521.

3. Wielpütz M, Kauczor HU: MRI of the lung: State of the art. *Diagnostic Interv Radiol* 2012:344–353.

4. Bajc M, Neilly JB, Miniati M, Schuemichen C, Meignan M, Jonson B: EANM guidelines for ventilation/perfusion scintigraphy : Part 1. Pulmonary imaging with ventilation/perfusion single photon emission tomography. *Eur J Nucl Med Mol Imaging* 2009; 36:1356–1370.

5. Thieme SF, Hoegl S, Nikolaou K, et al.: Pulmonary ventilation and perfusion imaging with dual-energy CT. *Eur Radiol* 2010; 20:2882–2889.

6. Kauczor HU, Wielpütz MO: *MRI of the Lung*. Second Ed. Springer Berlin Heidelberg; 2017. [*Medical Radiology*]

7. Wild JM, Marshall H, Bock M, et al.: MRI of the lung (1/3): Methods. *Insights Imaging* 2012; 3:345–353.

8. Heye T, Sommer G, Miedinger D, Bremerich J, Bieri O: Ultrafast 3D balanced steady-state free precession MRI of the lung: Assessment of anatomic details in comparison to low-dose CT. *J Magn Reson Imaging* 2015; 42:602–609.

9. Nyilas S, Bauman G, Sommer G, et al.: Novel Magnetic Resonance Technique for Functional Imaging Of Cystic Fibrosis Lung Disease. *Eur Respir J 2017* :[Article in

press].

10. Biederer J, Beer M, Hirsch W, et al.: MRI of the lung (2/3). Why ... when ... how? *Insights Imaging* 2012; 3:355–371.

11. Biederer J, Mirsadraee S, Beer M, et al.: MRI of the lung (3/3)—current applications and future perspectives. *Insights Imaging* 2012; 3:373–386.

12. Semelka RC, Balci NC, Wilber KP, et al.: Breath-hold 3D gradient-echo MR imaging of the lung parenchyma: Evaluation of reproducibility of image quality in normals and preliminary observations in patients with disease. *J Magn Reson Imaging* 2000; 11:195–200.

13. Ohno Y, Murase K, Higashino T, et al.: Assessment of bolus injection protocol with appropriate concentration for quantitative assessment of pulmonary perfusion by dynamic contrast-enhanced MR imaging. *J Magn Reson Imaging* 2007; 25:55–65.

14. Mortensen J, Gutte H: SPECT/CT and pulmonary embolism. *Eur J Nucl Med Mol Imaging* 2014; 41:81–90.

15. Biederer J, Both M, Graessner J, et al.: Lung morphology: fast MR imaging assessment with a volumetric interpolated breath-hold technique: initial experience with patients. *Radiology* 2003; 226:242–249.

16. Scheffler K, Lehnhardt S: Principles and applications of balanced SSFP techniques. *Eur Radiol* 2003; 13:2409–2418.

17. Bieri O: Ultra-fast steady state free precession and its application to in vivo 1H morphological and functional lung imaging at 1.5 tesla. *Magn Reson Med* 2013; 70:657–663.

18. Bauman G, Pusterla O, Bieri O: Ultra-fast Steady-State Free Precession Pulse

Sequence for Fourier Decomposition Pulmonary MRI. *Magn Reson Med* 2015:75:1647-53.

19. Pusterla O, Bauman G, Wielpütz MO, et al.: Rapid 3D in vivo 1H human lung respiratory imaging at 1.5 T using ultra-fast balanced steady-state free precession. *Magn Reson Med* 2016:. DOI: 10.1002/mrm.26503.

20. Pusterla O, Bauman G, Bieri O: Three-dimensional oxygen-enhanced MRI of the human lung at 1.5T with ultra-fast balanced steady-state free precession. *Magn Reson Med* 2017:n/a--n/a.

21. Huang T-Y, Huang I-J, Chen C-Y, Scheffler K, Chung H-W, Cheng H-C: Are TrueFISP images T2/T1-weighted? *Magn Reson Med* 2002; 48:684–688.

22. Jung B, Krombach GA, Gunther RW, Buecker A: Is postcontrast trueFISP imaging advantageous? *Invest Radiol* 2004; 39:517–523.

23. Pusterla O, Bauman G, Bieri O: Balanced SSFP pulmonary signal enhancement after contrast agent injection. Proc. Intl. Soc. Mag. Reson. Med. 24; 2016:2916.

24. Bauman G, Santini F, Pusterla O, Bieri O: Pulmonary relaxometry with inversion recovery ultra-fast steady-state free precession at 1.5T. *Magn Reson Med* 2017; 77:74–82.

25. Hatabu H, Gaa J, Kim D, Li W, Prasad P V, Edelman RR: Pulmonary perfusion: Qualitative assessment with dynamic contrast-enhanced MRI using ultra-short TE and inversion recovery turbo FLASH. *Magn Reson Med* 1996; 36:503–508.

26. Biederer J, Graessner J, Heller M: Magnetic resonance imaging of the lung with a volumetric interpolated 3D-Gradient echo sequence - Magnetresonanztomographie der Lunge mit einer volumeninterpolierten 3D-Gradientenechosequenz. *Fortschr Röntgenstr*

2001; 173:883–887.

27. Haacke E, Brown R, Thompson M, Venkatesan R: Magnetic resonance imaging: physical principles and sequence design. 1999. *New York A John Wiley Sons* 1999.

28. Klein S, Staring M, Murphy K, Viergever MA, Pluim JPW: Elastix: A toolbox for intensity-based medical image registration. *IEEE Trans Med Imaging* 2010; 29:196–205.

29. Bieri O: A Method for Visualization of Parenchyma and Airspaces from 3D Ultra-Fast Balanced SSFP Imaging of the Lung at 1.5T. Proc. Intl. Soc. Mag. Reson. Med. 22; 2014:2300.

30. Watson PF, Petrie A: Method agreement analysis: A review of correct methodology. *Theriogenology* 2010; 73:1167–1179.

31. Vanbelle S: A New Interpretation of the Weighted Kappa Coefficients. *Psychometrika* 2016; 81:399–410.

32. Johnson KM, Fain SB, Schiebler ML, Nagle S: Optimized 3D Ultrashort Echo Time Pulmonary MRI. *Magn Reson Med* 2013; 70:1241–1250.

33. Mugler III JP, Meyer C, Pfeuffer J, Stemmer A, Berthold K: Accelerated Stack-of-Spirals Breath-hold UTE Lung Imaging. Proc. Intl. Soc. Mag. Reson. Med. 25; 2017:4904.

34. Hopkins SR, Wielpütz MO, Kauczor H-U: Imaging lung perfusion. *J Appl Physiol* 2012; 113:328–39.

35. Hopkins SR, Henderson a C, Levin DL, et al.: Vertical gradients in regional lung density and perfusion in the supine human lung: the Slinky effect. *J Appl Physiol* 2007; 103:240–248.

36. Almquist HM, Palmer J, Jonson B, Wollmer P: Pulmonary perfusion and density gradients in healthy volunteers. *J Nucl Med* 1997; 38:962–966.

37. Bauman G, Bieri O: Reversed half-echo stack-of-stars TrueFISP (TrueSTAR). *Magn Reson Med* 2015:n/a--n/a.

38. Song T, Laine AF, Chen Q, et al.: Optimal k-Space Sampling for Dynamic Contrast-Enhanced MRI with an Application to MR Renography. *Magn Reson Med* 2009; 61:1242–1248.

39. Otsu N: A Threshold Selection Method from Gray-Level Histograms. *IEEE Trans Syst Man Cybern* 1979; 9:62–66.

40. Tustison NJ, Qing K, Wang C, Altes TA, Mugler JP: Atlas-based estimation of lung and lobar anatomy in proton MRI. *Magn Reson Med* 2015.

TABLES

TABLE 1. UfSSFP and VIBE pulse sequences parameters.

Parameter	**ufSSFP**	**VIBE**
TR/TE	1.43 / 0.61 ms	4.0 / 1.05 ms
Flip angle α	35°	10°
Bandwidth	1563 Hz/pixel	580 Hz/pixel
Acquisition plane	Coronal	Transversal
Field of View (FoV)	400×400×280 mm^3	280×400×360 mm^3
Matrix	160×160×112	112×160×112
Resolution	2.5×2.5×2.5 mm^3	2.5×2.5×3 mm^3 [a]
Slice resolution	100%	80%
Phase oversampling	30%	0
Phase partial Fourier	8/8 (6/8) [b]	6/8
Slice partial Fourier	8/8	6/8
GRAPPA factor	2	2
Acquisition time	15 s (11 s) [b]	17 s

[a] Interpolated to 1.25×1.25×3 mm^3.

[b] Acquisition time can be shortened by technicians for patient examination, if necessary.

TABLE 2. Comparison of the observed signal enhancement ratio (SER) for ufSSFP and VIBE for different anatomical regions and averaged over ten subjects from the control group (healthy lung).

SER, mean ± intersubject SD (pooled intrasubject SD) [%]

	Lung	*Aorta*	*Liver*	*Muscle*	*Fat*
ufSSFP	99 ± 9 (23)	81 ± 7 (8)	33 ± 8 (12)	26 ± 5 (6)	2 ± 1 (4)
VIBE	47 ± 12 (27)	164 ± 17 (21)	36 ± 8 (5)	22 ± 3 (5)	7 ± 4 (3)

TABLE 3. Artifact evaluation (e.g. pulsation, heart-beating, partial volume effects) per lung lobe for ufSSFP-SER and VIBE-SER in ten subjects from the control group. “No artifact” is scored 0; score 1 indicates that 1-25% of the lobe volume is affected by artifacts; score 2, 26-50%; score 3, 51-75 %; and score 4, 76-100%. No scores above 2 were found for ufSSFP; artifacts in the lower lobes and the lingula are attributable to cardiac pulsation. Average score of the artifacts: 2.3±0.6 for VIBE-SER and 0.6±0.4 for ufSSFP-SER.

Abbreviations: RU = right-upper lobe; RM = right-middle; RL = right-lower; LU = left-upper; Lin = lingula; LL = left-lower.

Image artifacts for ufSSFP-SER and VIBE-SER divided by lung lobe (n=10 subjects).

ufSSFP-SER

	RU	RM	RL	LU	Lin	LL
No artifacts	10	7	6	9	4	-
Score 1	-	1	4	1	4	5
Score 2	-	2	-	-	2	5
Score 3	-	-	-	-	-	-
Score 4	-	-	-	-	-	-

VIBE-SER

	RU	RM	RL	LU	Lin	LL
No artifacts	-	1	-	-	2	-
Score 1	-	-	2	-	1	2
Score 2	2	7	6	3	5	5
Score 3	5	1	2	6	2	3
Score 4	3	1	-	1	-	-

FIGURES

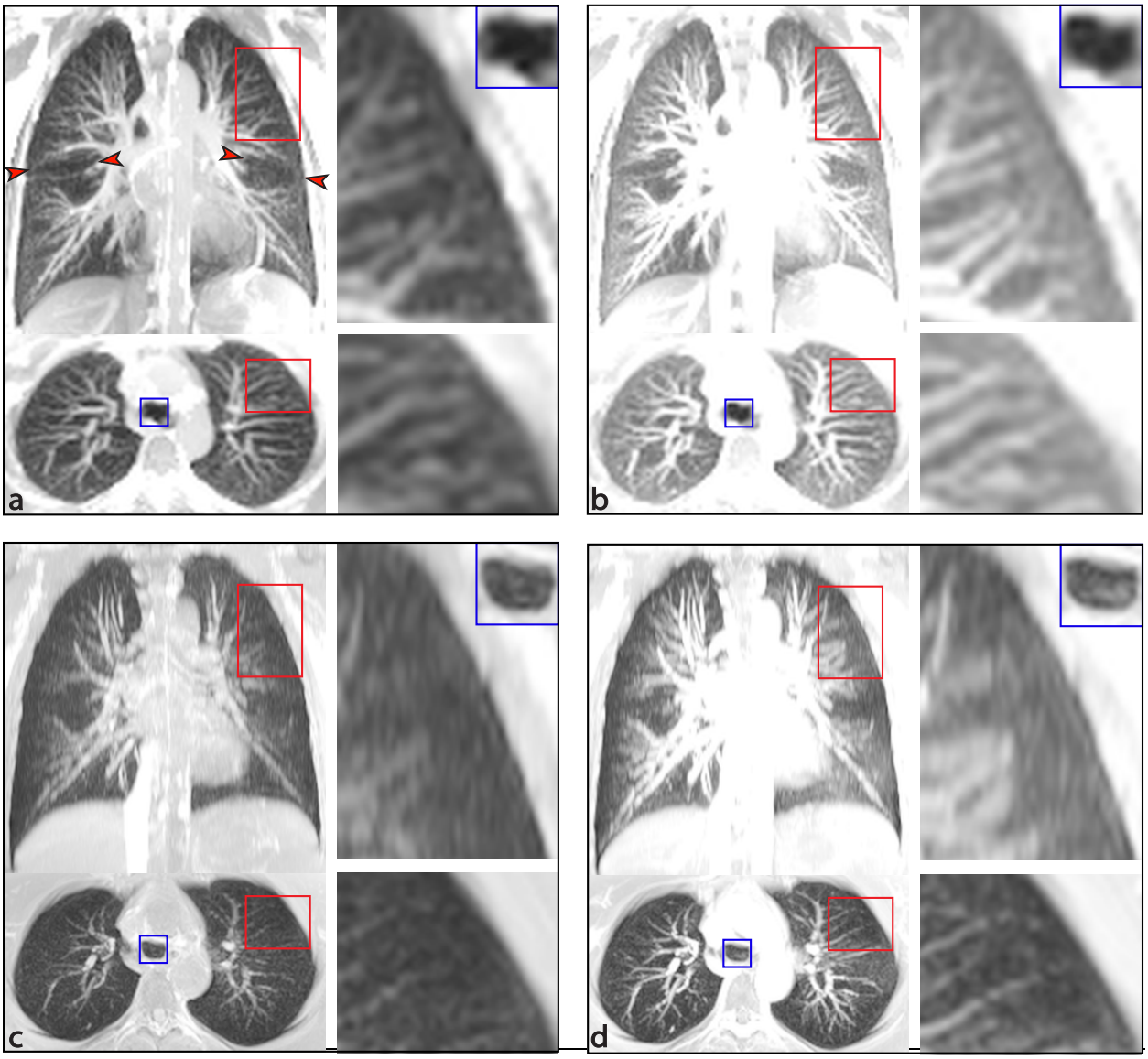

FIGURE 1: Maximum intensity projection (effective slice thickness 25 mm) of ufSSFP (a, b) and VIBE (c, d) before (a, c) and after contrast agent injection (b, d) in a 26-year-old male subject from the control group. The red rectangles indicate regions of interests in the lungs, “zoomed” on the right of the figures; in blue is marked the trachea, “zoomed” on the top-right of the figures. For visual comparison of the signal increase after contrast administration, the same windowing (logarithmic grey-scale) is used for

pre- and post-contrast images [(a, b) and (c, d)]. Both sequences allow for the depiction of the pulmonary vasculature. The red arrowheads (a) indicate exemplarily the fissure between the lung lobes [observable in all images a-d].

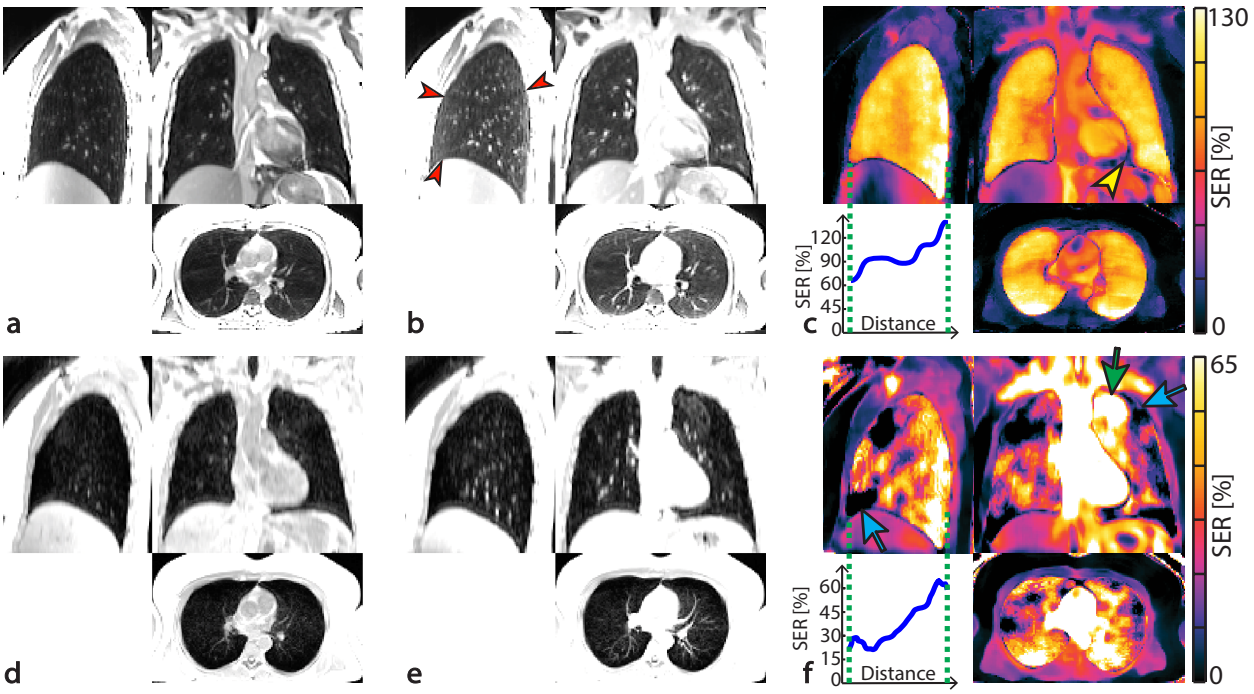

FIGURE 2: Comparison of ufSSFP (a-c) and VIBE (d-f) for a representative subject from the control group (female, 54 years old). Native (non-registered) pre-contrast (a, d) and post-contrast datasets (b, e) are co-registered and median-filtered to calculate signal enhancement ratio maps (c, f). The same windowing (grey-scale) is used for pre- and post-contrast images [(a, b) and (d, e)] for visual comparison of the signal increase after i.v. contrast administration. SER images with ufSSFP appear homogeneous in the lung [(c), SER=96%±23%, cv=24%], whereas VIBE-based SER images show patchy hyper- and hypo-intense artifacts (e.g. green and blue arrows) [(f), SER=41%±28%, cv=86%]. SER values in the lung increase from ventral to dorsal, as depicted in the plots [see left-lower panel in (c, f)] which report the mean SER in the iso-gravitational

planes as a function of the ventral-to-dorsal distance. Balanced SSFP “banding” artifacts are entirely mitigated by the accelerated ufSSFP acquisition scheme (a, b). Different scaling was used for ufSSFP-SER and VIBE-SER images in (c, f); in (c), the yellow arrowhead shows exemplarily an artefact caused by heart pulsation. In both VIBE and ufSSFP images the fissures between the lung lobes are observable [e.g. sagittal view in (b), marked by red arrowheads].

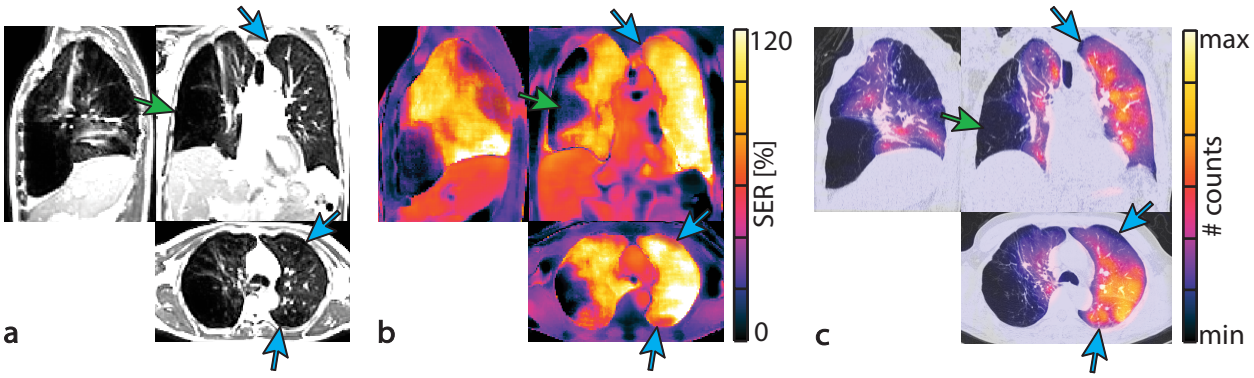

FIGURE 3: Side-by-side comparison of post-contrast ufSSFP (a), ufSSFP-SER (b), and ^{99m}Tc-MAA SPECT/CT fusion images (c) in a 61-year-old male patient with COPD GOLD II and emphysema. There is an extensive destruction of the right lung of this patient by emphysema with large confluent bullae (green arrows). Reduced SER is also seen in the emphysematous regions in the left lung (blue arrows) with apical predominance. Spatial coincidence is observed between areas of low SER in ufSSFP and areas of low radiotracer uptake in ^{99m}Tc-MAA SPECT. The whole lung SER was 75%±42% (mean±SD).

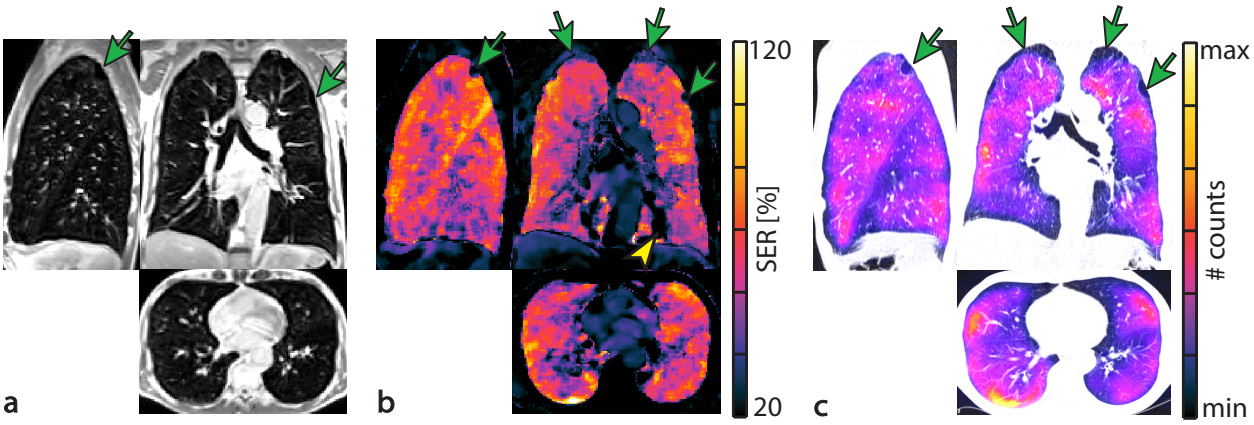

FIGURE 4: Comparison of post-contrast ufSSFP (a), ufSSFP-SER (b), and ^{99m}Tc-MAA SPECT/CT fusion images (c) in a 70-year-old male patient with COPD GOLD IV. In this patient, a more uniform distribution of emphysema compared to the patients presented in Figure 3 and Supporting Figure S5 was observed. A homogenous but still patchy decrease in SER is noted (whole lung SER = 57%±28%, mean±SD). Again there is a good visual agreement between ufSSFP-SER imaging and SPECT/CT, e.g. in the regions of bullous emphysema in the apices (green arrows). In (b), a pulsation artefact from the heart is indicated by the yellow arrowhead.

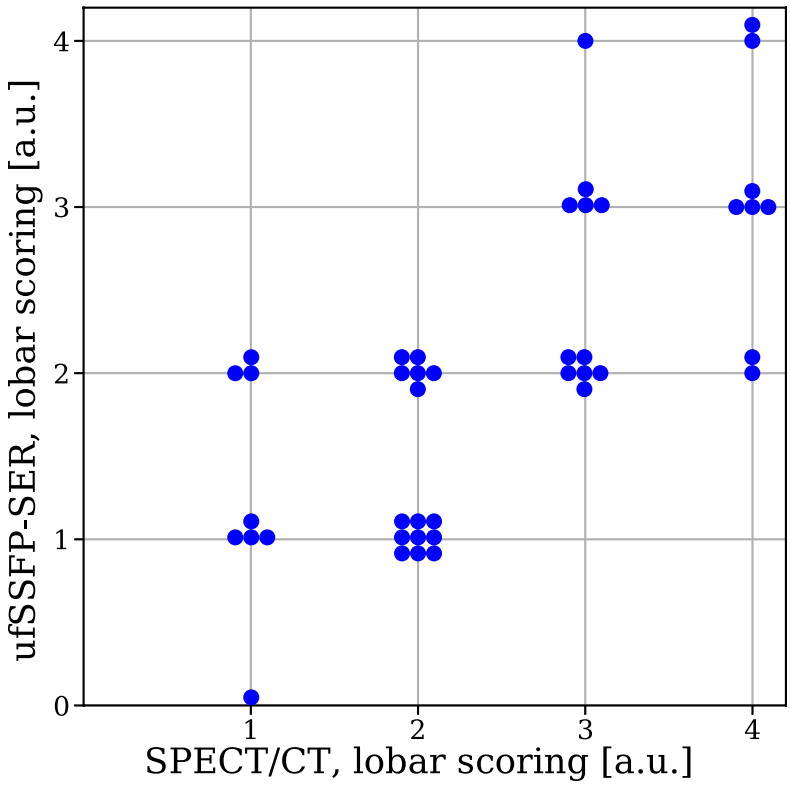

FIGURE 5: Functional defects per lung lobe in seven COPD patients evaluated with ufSSFP-SER and with ^{99m}Tc-MAA SPECT/CT. Score 0 indicates no defects; score 1, 1-25% of lobe volume is affected; score 2, 26-50%; score 3, 51-75%; score 4, 76-100%. The lobar scoring for the two imaging modalities differed up to 2 units and showed moderate intermodality agreement with SPECT/CT (Cohen's kappa κ_l=0.41, κ_q = 0.64).

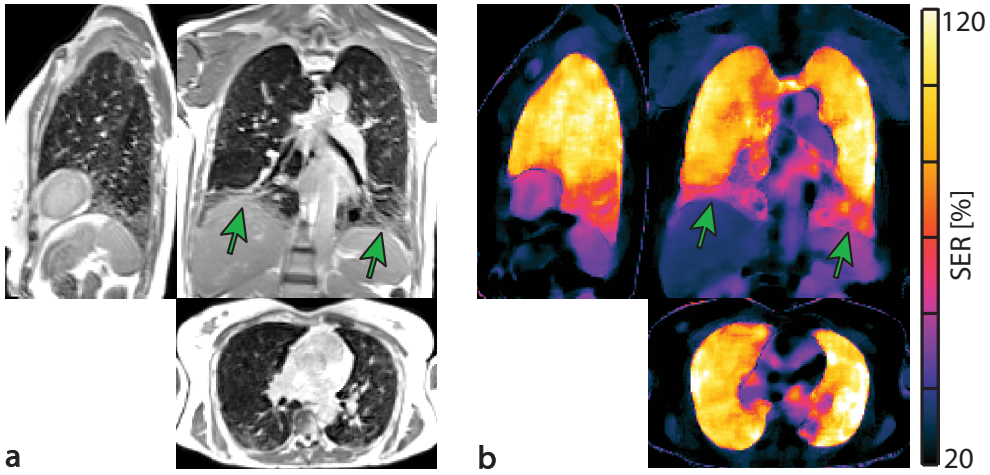

FIGURE 6: Post-contrast ufSSFP images (a), and ufSSFP-SER images (b) in a 58-year-old female patient with scleroderma and NSIP. A streaky decrease in SER is noted in both lower lobes corresponding to fibrotic changes seen on morphological MRI (green arrows).

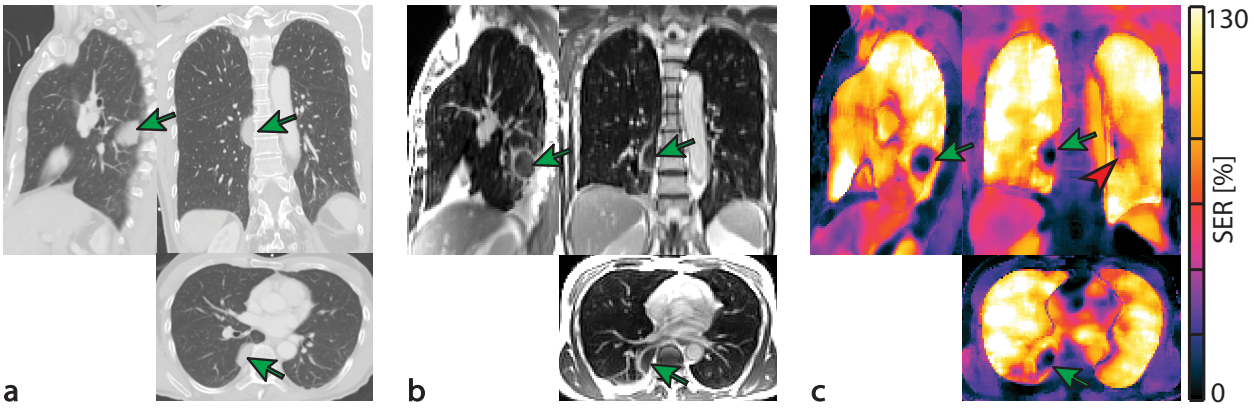

FIGURE 7: CT (a), post-contrast ufSSFP (b), and ufSSFP-SER images (c) in a 71-year-old male patient after traumatic lung injury. The green arrow indicates a subpleural hematoma in the lung parenchyma of the right lower lobe. In the SER images (c), in comparison to the normal lung (SER=110%±27%, mean±SD) the hematoma shows a

reduced enhancement (SER=34%±23%, mean±SD). The red arrowhead on the SER map (coronal view) indicates an artefact caused by pulsation.

SUPPORTING FIGURES

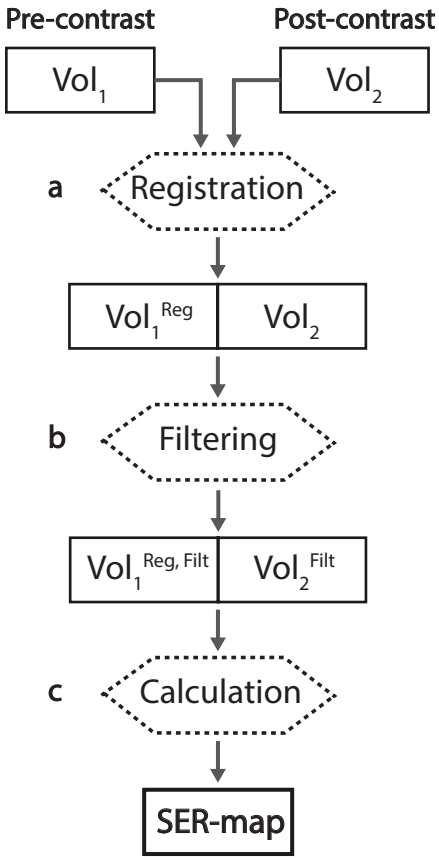

a) Registration spatially matches structures
b) Median filtering removes vasculature
c) $(Vol_2^{Filt} - Vol_1^{Reg, Filt}) \cdot (Vol_1^{Reg, Filt})^{-1}$

Supporting Figure S1. Schematic of the post-processing for signal enhancement ratio (SER) imaging. Pre-contrast (Vol_1) and post-contrast (Vol_2) volumetric datasets are first registered (a) to match the lung structures (e.g. diaphragm positions and vessels). Successively, the datasets are median filtered (b) to remove vasculature and to get access to the parenchymal signal. (c) Pulmonary SER-maps are finally calculated (see "Method" section).

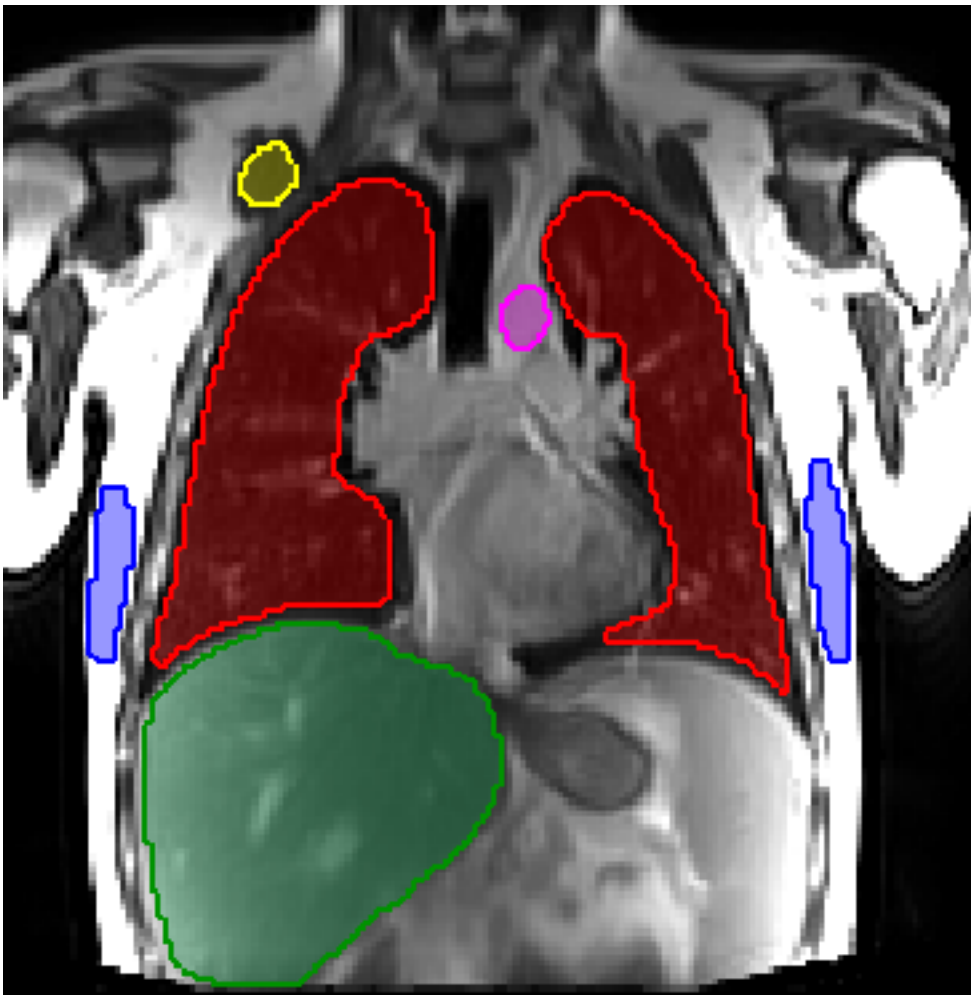

Supporting Figure S2. Exemplary ufSSFP coronal view indicating representative volumetric region of interests of the lung (depicted in red, volume = 2716 cm^3), aortic arch (pink, 21 cm^3), liver (green, 1322 cm^3), muscle (yellow, 174 cm^3) and fat (blue, 125 cm^3).

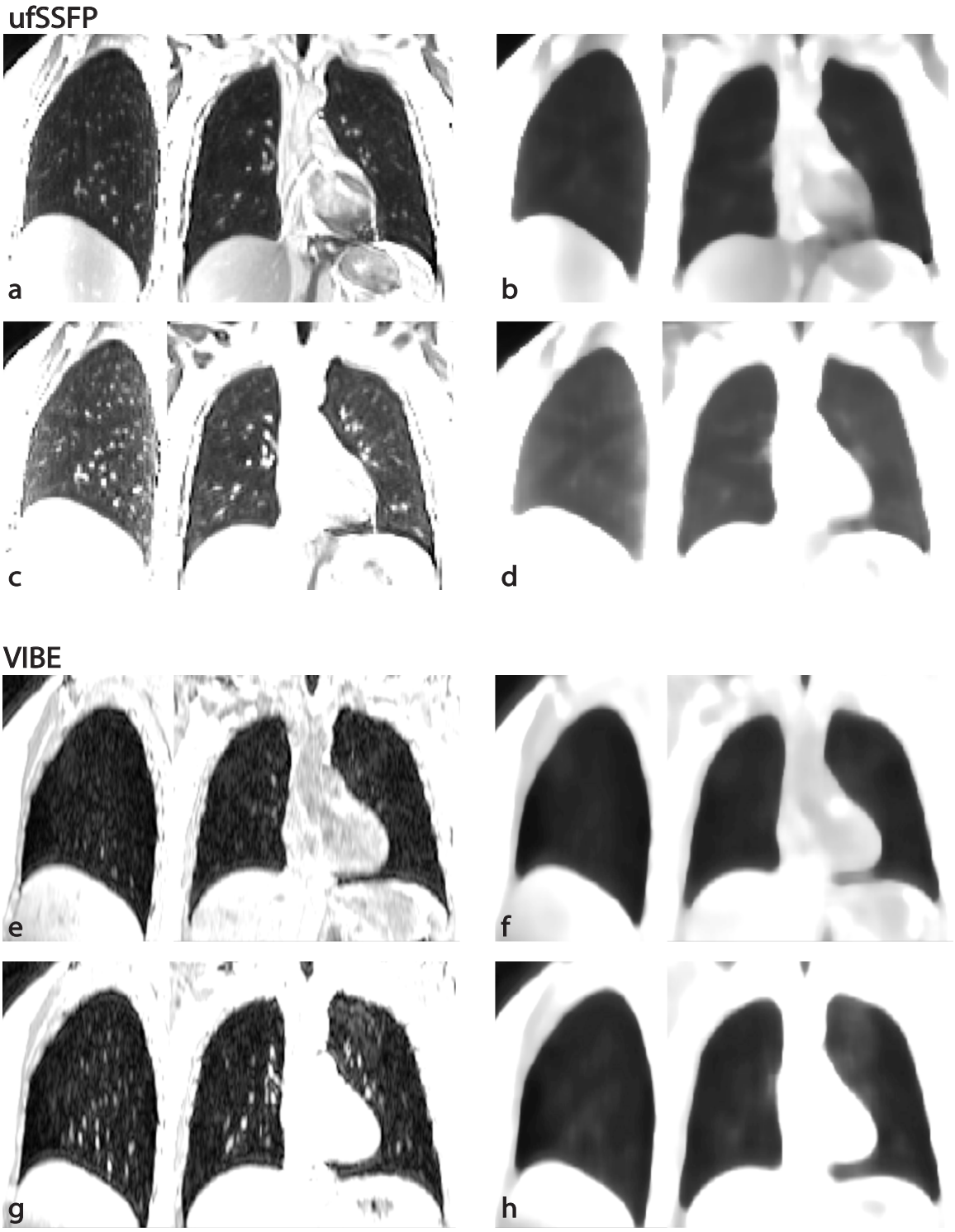

Supporting Figure S3. UfSSFP (a-d) and VIBE (e-h) native images (a, c, e, g) and median filtered (b, d, f, h) before (a, b, e, f) and after contrast agent injection (c, d, g, h) in a 54-year-old female subject from the control group. Median filtering removes

vasculature, small airways and noise to recover the underlying smooth parenchymal-background signal variation. The same windowing (greyscale) was used in (a-d) and (e-h).

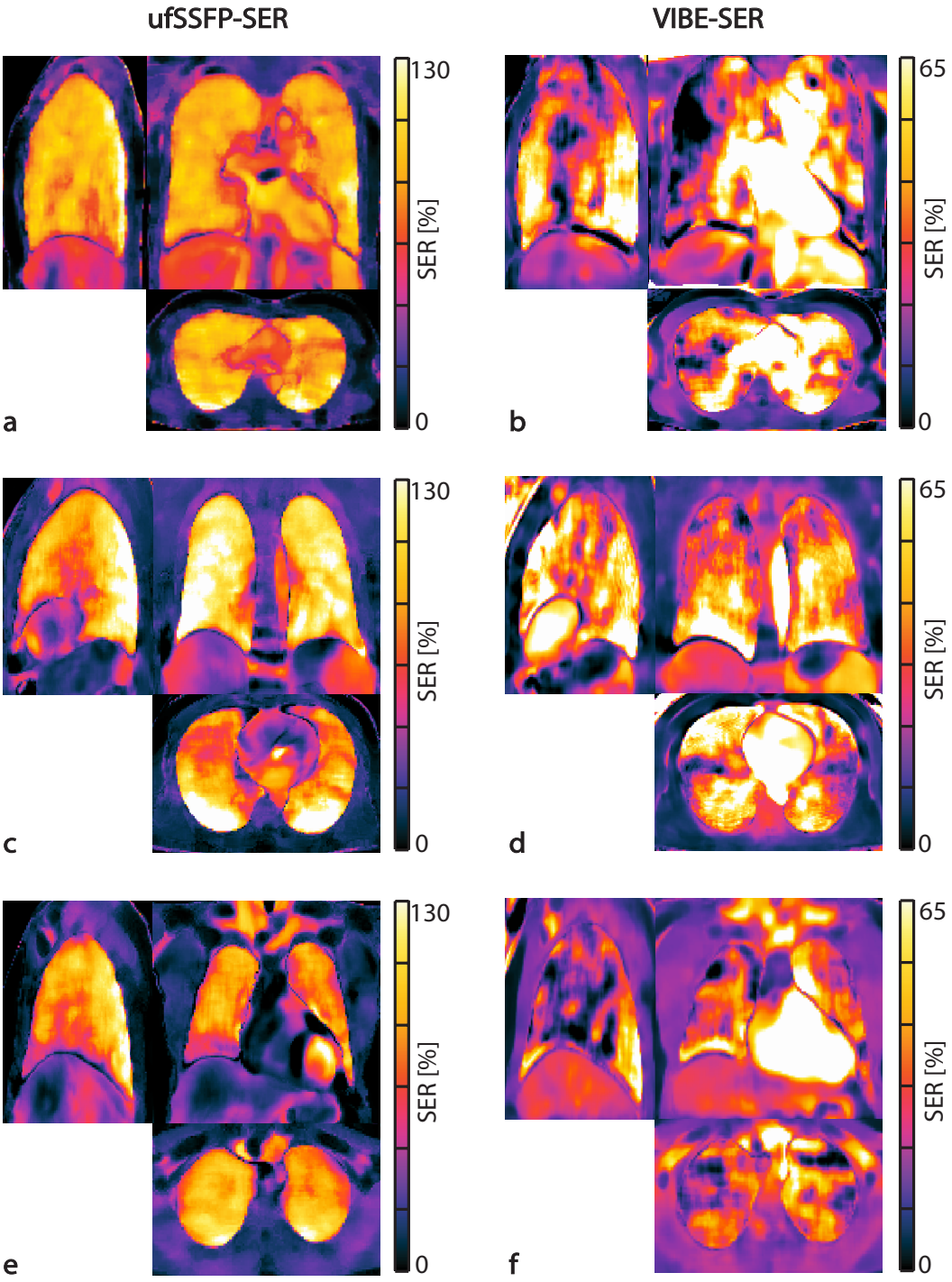

Supporting Figure S4. Side-by-side comparison of signal enhancement ratio imaging with ufSSFP (a, c, e) and VIBE (b, d, f) in three subjects with no lung disease from the control group [(a, b) female 52 years old, (c, d) male 28 years old, and (e, f) male 43 years old]. To note, the color maps for ufSSFP and VIBE SER are differently scaled. The SER in the lung is more homogeneous using ufSSFP than using VIBE (cf. Table 2). Whole lung mean SER values were 97%±20% [(a), mean±SD], 116%±27% (c), 101%±25% (e) for ufSSFP; 55%±24% (b), 61%±31% (d), and 55%±27% (f) for VIBE. To note, in the region of the heart, due to pulsation (and thus partial-volume effects in the native images) the SER values have large signal variations [cf. sagittal view in (c)].

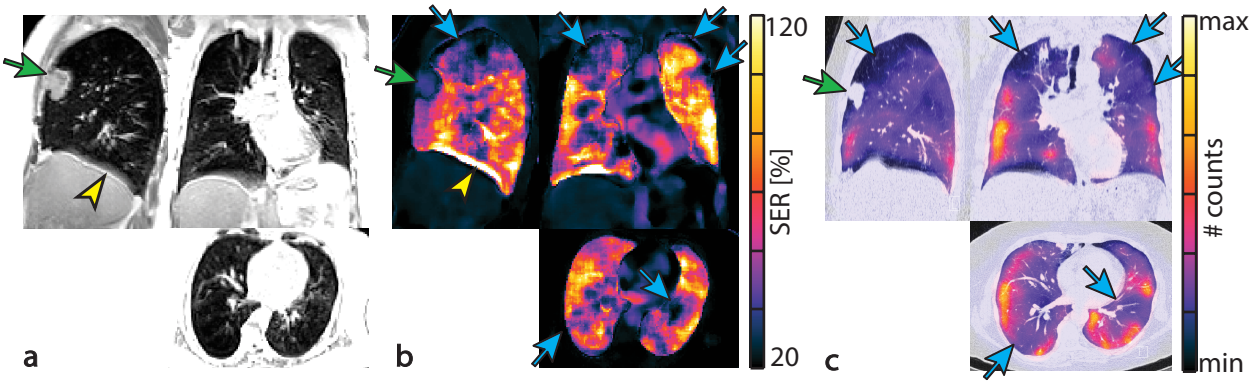

Supporting Figure S5. Comparison of post-contrast ufSSFP (a), ufSSFP-SER (b), and ^{99m}Tc-MAA SPECT/CT fusion images (c) in a 57-year-old female patient with COPD GOLD III and an NSCLC in the right upper lobe (green arrows). There is extensive inhomogeneity of SER in the lung parenchyma of this patient due to COPD (exemplary impairments depicted by blue arrows) with spatial coincidence of the defects observed with ufSSFP-SER and ^{99m}Tc-MAA-SPECT. The whole lung SER was 68%±24% (mean±SD). To note, the solid tumor in the right upper lobe of this patient shows lower SER than the surrounding lung parenchyma (43%±8%). In (b), the SER scale was

optimized to facilitate visualizations of functional impairments. The yellow arrowheads in (a, b) indicate a blurring artifact, caused by a minute diaphragm movement due to non-perfect breath-holding during imaging.